Vansco, M. F., Marchetti, B., & Lester, M. I. (2018). Electronic spectroscopy of methyl vinyl ketone oxide: A four-carbon unsaturated Criegee intermediate from isoprene ozonolysis: A four-carbon unsaturated Criegee intermediate from isoprene ozonolysis. *Journal of Chemical Physics*, *149*(24), [244309]. https://doi.org/10.1063/1.5064716

Electronic spectroscopy of methyl vinyl ketone oxide: A four-carbon unsaturated Criegee intermediate from isoprene ozonolysis

Michael F. Vansco 🆔, Barbara Marchetti, and Marsha I. Lester 🆔

View Online   **Export Citation**   **CrossMark**

ARTICLES YOU MAY BE INTERESTED IN

Electronic spectroscopy of methyl vinyl ketone oxide: A four-carbon unsaturated Criegee intermediate from isoprene ozonolysis

Michael F. Vansco, Barbara Marchetti, and Marsha I. Lester[a)]
Department of Chemistry, University of Pennsylvania, Philadelphia, Pennsylvania 19104-6323, USA

Ozonolysis of isoprene, one of the most abundant volatile organic compounds in the atmosphere, proceeds through methyl vinyl ketone oxide (MVK-oxide), methacrolein oxide, and formaldehyde oxide (CH_2OO) Criegee intermediates. The present study focuses on MVK-oxide, a four-carbon unsaturated carbonyl oxide intermediate, using vacuum ultraviolet photoionization at 118 nm and UV-visible induced depletion of the m/z = 86 mass channel to characterize its first $\pi^* \leftarrow \pi$ electronic transition. The electronic spectrum is broad and unstructured with its peak at 388 nm (3.2 eV). The MVK-oxide spectrum is shifted to a significantly longer wavelength than CH_2OO and alkyl-substituted Criegee intermediates studied previously due to extended conjugation across the vinyl and carbonyl oxide groups. Electronic excitation results in rapid dissociation at $\lambda \leq 430$ nm to methyl vinyl ketone and O ^1D products, the latter detected by 2 + 1 resonance enhanced multiphoton ionization using velocity map imaging. Complementary electronic structure calculations (CASPT2(12,10)/AVDZ) predict two $\pi^* \leftarrow \pi$ transitions with significant oscillator strength for each of the four conformers of MVK-oxide with vertical excitation energies (and corresponding wavelengths) in the 3.1-3.6 eV (350-400 nm) and 4.5-5.5 eV (220-280 nm) regions. The computed electronic absorption profile of MVK-oxide, based on a Wigner distribution of ground state configurations and summed over the four conformers, is predicted to peak at 397 nm. UV-visible spectroscopy on the first $\pi^* \leftarrow \pi$ transition is shown by a combination of experiment and theory to provide a sensitive method for detection of the MVK-oxide Criegee intermediate that will enable further studies of its photochemistry and unimolecular and bimolecular reaction dynamics. *Published by AIP Publishing.*
https://doi.org/10.1063/1.5064716

I. INTRODUCTION

Alkenes are important unsaturated hydrocarbon species that are introduced into the atmosphere from both anthropogenic and biogenic sources. Among these, isoprene (2-methyl-1,3-butadiene, $CH_2{=}C(CH_3){-}CH{=}CH_2$) with global emissions on the order of 500 Tg/yr,[1] primarily from foliar sources, is the most abundant nonmethane volatile organic compound in the Earth's troposphere. Isoprene and other alkenes are removed from the atmosphere through their reactions with the hydroxyl radical (OH), ozone (O_3), and the nitrate radical (NO_3, nighttime only).[2–4] Here, we focus on alkene ozonolysis, which proceeds by ozone addition across the olefinic double bond to yield a primary ozonide (POZ).[5] The POZ rapidly decomposes to form energized carbonyl (e.g., aldehydes or ketones) and carbonyl oxide species, the latter known as the Criegee intermediate. The resultant Criegee intermediate can undergo unimolecular decay to OH radicals and other products,[6–9] and/or bimolecular reaction with atmospheric species, including water vapor and SO_2,[10–16] which may lead to aerosol formation and impact on climate.[17]

Ozonolysis of isoprene can occur at two distinct double bond locations. Due to the asymmetry of each double bond site, ozonolysis at the $C_{(1)}{=}C_{(2)}$ bond results in a POZ that generates methyl vinyl ketone oxide (($CH_2{=}CH)(CH_3)COO$, MVK-oxide) with formaldehyde, as shown in Scheme 1, or formaldehyde oxide (CH_2OO) with methylvinylketone (($CH_2{=}CH)(CH_3)CO$, MVK).[18–21] Ozonolysis at the $C_{(3)}{=}C_{(4)}$ bond yields a different POZ and forms methacrolein oxide (($CH_2{=}C(CH_3))CHOO$, MACR-oxide) with formaldehyde or CH_2OO with methacrolein (($CH_2{=}C(CH_3))CHO$, MACR). Very little is known about the four-carbon unsaturated MVK-oxide and MACR-oxide species, which are estimated to account for 23% and 19% of the Criegee intermediates formed in isoprene ozonolysis, respectively.[21,22]

A new synthetic route was introduced in 2012 that enabled direct experimental investigation of CH_2OO and simple alkyl-substituted Criegee intermediates.[23,24] In this method, a *gem*-diiodo alkane precursor is photolyzed to produce a monoiodo alkyl radical, which subsequently reacts with O_2 to produce the Criegee intermediate. Unfortunately, analogous *gem*-diiodo precursors cannot be readily synthesized to produce the four-carbon unsaturated Criegee intermediates. Recently, this laboratory demonstrated that photolysis of 1,3-diiodobut-2-ene generates a resonance-stabilized monoiodoalkene radical that reacts with O_2 to produce MVK-oxide.[25] Thus far, MVK-oxide has been characterized by infrared action spectroscopy

---
a)Author to whom correspondence should be addressed: milester@sas.upenn.edu
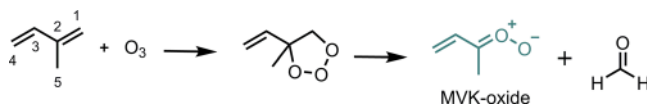
SCHEME 1. Ozonolysis of isoprene proceeds via a primary ozonide to methyl vinyl ketone oxide (MVK-oxide) and formaldehyde products.

with detection of OH products arising from unimolecular decay.[25] Here, we report the UV-visible (vis) absorption spectrum of MVK-oxide and present initial results on its photochemistry.

The characteristic UV absorption of Criegee intermediates is of great importance as a sensitive detection technique for laboratory studies of their bimolecular reactions with atmospheric species. For example, UV absorption of CH_2OO was utilized to reveal its substantive rate of removal and quadratic dependence on water vapor concentration.[12,15] The very strong UV transitions of prototypical Criegee intermediates with oscillator strength on the order of $f \sim 0.1$ involve a $\pi^* \leftarrow \pi$ transition associated with the four π electrons of the carbonyl oxide $(C{=}O^+O^-)$ group with zwitterionic character.[26–30] The UV spectra are peaked at 335 nm for CH_2OO,[27,31,32] ca. 320 nm for syn-CH_3CHOO,[28,33,34] $(CH_3)_2COO$ and CH_3CH_2CHOO,[29,35] and ca. 360 nm for the less stable $anti$-conformer of CH_3CHOO.[33] In general, the UV spectra of the Criegee intermediates are relatively broad and unstructured due to rapid dissociation in the excited electronic state, although CH_2OO exhibits some structure in the long wavelength tail region attributed to vibrational resonances.[36,37] The excited electronic state accessed upon UV excitation of the Criegee intermediates couples via conical intersections to multiple repulsive potentials that produce O ^1D fragments and associated singlet carbonyl co-products in the lowest spin-allowed channel.[30,36,38]

Here, we provide a detailed experimental and theoretical examination of the UV-vis spectrum of MVK-oxide, which should enable sensitive spectroscopic detection of MVK-oxide for laboratory studies of its photochemistry, and unimolecular and bimolecular reactions. MVK-oxide is distinctly different than previously studied Criegee intermediates because the associated vinyl group couples to the carbonyl oxide group to extend the π-conjugation that then involves six π electrons. MVK-oxide is predicted to have four conformational forms with stabilities that differ by only 3 kcal mol^{-1}, yet significant barriers separate the conformers and restrict interconversion between them.[19,25] The four conformers of MVK-oxide are labeled as syn or $anti$, depending on the orientation of the methyl group with respect to the terminal O atom, and cis or $trans$, designating the relative orientation of the C=C and C=O double bonds. The four conformers of MVK-oxide are expected to be populated, and they have similar and potentially overlapping UV-vis spectra.

The UV spectra of simple Criegee intermediates have been recorded using a variety of techniques including direct absorption,[32,33,39] UV action spectroscopy with O-atom detection,[40,41] and UV-induced depletion of the associated VUV (vacuum ultraviolet) photoionization signal.[27–29] Here, we demonstrate 10.5 eV photoionization of MVK-oxide and detection on the parent m/z = 86 mass channel. Next, we obtain

a UV-vis spectrum of MVK-oxide through UV-vis induced depletion of the photoionization signal and compare with a high-level calculation of the absorption spectra for the four MVK-oxide conformers and other relevant isomeric species. Finally, we examine the UV-vis induced dissociation dynamics of the MVK-oxide conformers to MVK X $^1A'$ + O ^1D products, again comparing with theoretical calculations of their relative stabilities, electronic transitions, and asymptotic energies.

II. THEORETICAL METHODS AND RESULTS

In a previous study,[25] ground state optimizations were carried out for the four conformers of MVK-oxide using the B2PLYP-D3/VTZ method and basis[42–44] as implemented in Gaussian 09.[45] The zero-point corrected energies of the four conformers were evaluated using the ANL0-B2F method (a slightly modified version of the ANL0-F12 approach).[46] The relative energies and optimized structures are given in Table S1 and Fig. S1. In addition, vertical and adiabatic ionization energies of the four conformers were calculated at the coupled-cluster single double triple [CCSD(T)]-F12/CBS(TZ-F12,QZ-F12)//B2PLYP-D3/VTZ level of theory and are listed in Table I.

In this work, electronic excitation energies and oscillator strengths are calculated using the Complete Active Space with Second Order Perturbation Theory (CASPT2)[47–49] coupled with Dunning's augmented correlation consistent basis set of double-ζ (AVDZ)[50] for the lowest six singlet electronic transitions. The calculations are carried out using MOLPRO v2010.1.[51] The CASPT2 calculations are based on a seven-singlet state-averaged Complete Active Space-Self Consistent Field (SA7-CASSCF) reference wave function and involve an active space of 12 electrons in 10 orbitals. The occupied orbitals consist of three delocalized π orbitals, a $2p$ lone pair orbital localized on the oxygen atoms, and two σ orbitals arising from overlap of the in-plane oxygen orbitals. The unoccupied orbitals are two π^* orbitals that are delocalized across the whole molecule, and the σ^* and $3s$ Rydberg orbitals of the O atom. The first and second π^* orbitals are molecular orbitals nominally associated with the carbonyl oxide and vinyl

TABLE I. Vertical excitation energies (VEE, eV), corresponding wavelengths (λ, nm), and oscillator strengths (f) computed at the CASPT2(12,10)/AVDZ level of theory for electronic transitions of the four conformers of MVK-oxide to the $1^1\pi\pi^*$ and $2^1\pi\pi^*$ states. Vertical and adiabatic ionization energies (VIE and AIE, eV) evaluated at the CCSD(T)-F12/CBS(TZ-F12,QZ-F12)//B2PLYP-D3/cc-pVTZ level of theory from Ref. 25.

Conformer	VEE/eV (λ/nm)	f	VIE (AIE) (eV)
$anti$-cis	3.31 (375)	0.070	8.80 (8.65)
	4.68 (265)	0.043	
$anti$-$trans$	3.16 (392)	0.211	8.65 (8.54)
	5.55 (223)	0.345	
syn-cis	3.25 (381)	0.111	8.66 (8.55)
	4.52 (274)	0.091	
syn-$trans$	3.54 (350)	0.147	8.96 (8.61)
	4.52 (274)	0.109	

groups, respectively. Selected orbitals of the four conformers of MVK-oxide are shown in Fig. 1, while the full set of orbitals utilized in the active space for the CASSCF/CASPT2 calculations are depicted in Fig. S2. The first and second π^* orbitals are involved in the two optically bright $\pi^* \leftarrow \pi$ transitions that are the focus of the present theoretical study.

CASPT2(12,10)/AVDZ vertical excitation energies and oscillator strengths (f) are evaluated for the lowest six singlet electronic transitions of the four conformers of MVK-oxide (Table S2). The oscillator strengths (f_{ij}) for the spin allowed transitions are calculated using the CASSCF transition dipole moments (μ_{ij})[52]

$$f_{ij} = \frac{2}{3} E_{ij} \sum_{a=x,y,z} |\mu_{ij}|^2_\alpha$$

associated with electronic transitions from initial (i) to final (j) states with CASPT2 energies E_{ij}. The lowest excited electronic state ($1^1 n\pi^*$) with $n\pi^*$ character has negligible oscillator strength and is optically dark.

The next electronic state ($1^1 \pi\pi^*$) of $\pi\pi^*$ character is predicted to have significant oscillator strength in MVK-oxide, ranging from 0.07 for *anti-cis* to 0.21 for *anti-trans* (Table I and Table S2), as found for the prototypical Criegee intermediates studied previously.[26–28,53] The vertical excitation energies (Table I, Fig. 2) for transitions to the $1^1 \pi\pi^*$ states of the four conformers of MVK-oxide are computed at ~3.2–3.5 eV, corresponding to 390–350 nm. As a result, the first strong $\pi^* \leftarrow \pi$ transitions for the MVK-oxide conformers are expected at considerably lower energy/longer wavelength than the observed transitions for CH_2OO and alkyl-substituted Criegee intermediates. A similar spectral shift to longer wavelength was recently predicted for a model vinyl-substituted Criegee intermediate.[53]

A higher electronic $\pi^* \leftarrow \pi$ transition is predicted to have even larger oscillator strength for one conformer, specifically 0.35 for the *anti-trans* conformer. Vertical excitation on the
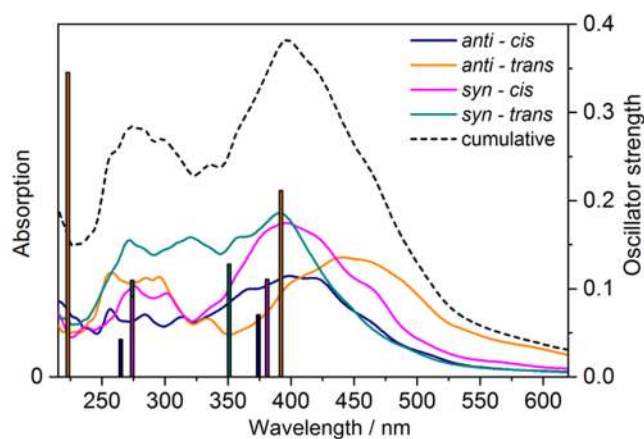
FIG. 2. Computed vertical electronic transitions and oscillator strengths to the $1^1\pi\pi^*$ and $2^1\pi\pi^*$ states of the four conformers of MVK-oxide (vertical bars) at the CASPT2(12,10)/AVDZ level of theory. Electronic absorption spectra (solid curves) based on a harmonic-oscillator Wigner distribution of ground state configurations are shown for *anti-cis* (blue), *anti-trans* (orange), *syn-cis* (purple), and *syn-trans* (cyan) conformers of MVK-oxide. The cumulative MVK-oxide electronic spectrum (dashed black curve) is the sum of the four conformer spectra, assuming equal ground state populations, but reduced in scale by a factor of 1.5.

second $\pi^* \leftarrow \pi$ transitions of the four conformers of MVK-oxide are predicted to occur at ~4.5–5.5 eV, corresponding to ~223–274 nm (Table I, Fig. 2). Experimental studies to $2^1\pi\pi^*$ states will be presented in a future publication. Additional excited electronic states of $n3s$, $n\pi^*$, and $\pi3s$ characters are predicted toward higher energy (Table S2), but in general have much weaker oscillator strength.

UV-vis absorption profiles for the two strong $\pi^* \leftarrow \pi$ transitions of the four conformers of MVK-oxide are then simulated using an approach similar to that implemented in Newton-X.[54–58] For each conformer, an ensemble of 300 (N) initial geometries is sampled using a Wigner distribution based on the ground state normal mode harmonic frequencies [calculated with B3LYP functional[59] and 6-311+G(d,p) basis set[60] using Gaussian09[45]]. The vertical excitation energies and oscillator strengths for the two $\pi^* \leftarrow \pi$ transitions are evaluated for each of the N initial geometries using CASPT2(10,8)/AVDZ. A Lorentzian line shape function with a broadening factor of 0.25 eV is assumed for each transition. The simulated absorption spectra for the four conformers of MVK-oxide are obtained by summing the intensities of the broadened transitions in the ensemble.

The resultant absorption spectra computed for the four conformers of MVK-oxide are shown in Fig. 2, along with a cumulative absorption profile for MVK-oxide obtained by summing the spectra of the four conformers assuming equal population (reduced in scale by a factor of 1.5 in Fig. 2). Figure S3 illustrates the ensemble of vertical transitions originating from the 300 N initial configurations that contribute to the absorption bands associated with the $1^1\pi\pi^*$ and $2^1\pi\pi^*$ states of the *syn-trans* conformer. The ensemble of individual transitions shows that the breadth of the two absorption bands for each conformer originates primarily from the Franck-Condon profiles associated with the N initial ground state configurations sampled. The simulated spectra are predicted to have maxima at 391 nm (*syn-trans*), 396 nm (*syn-cis*), 399 nm
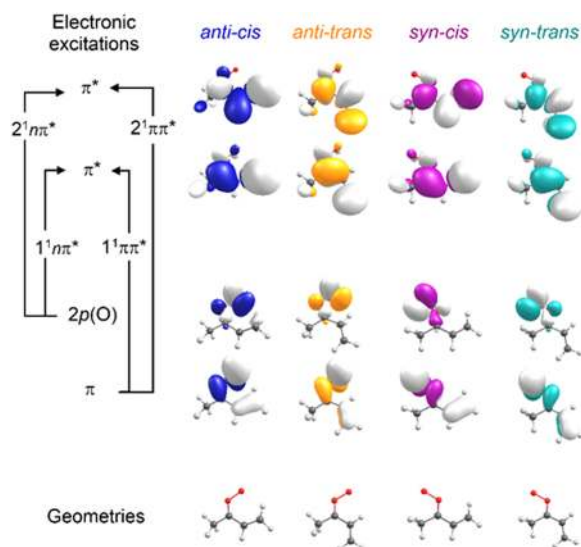

FIG. 1. Selected orbitals utilized in the active space for CASSCF/CASPT2 calculations of vertical excitation energies for electronic transitions of the four conformers of MVK-oxide. The arrows illustrate orbital promotions involved in forming the designated excited singlet states of MVK-oxide.

(*anti-cis*), and 440 nm (*anti-trans*). The cumulative spectrum for MVK-oxide is predicted to peak at 397 nm. Transitions to the $2^1\pi\pi^*$ states of the four MVK-oxide conformers are predicted to occur in the 225-325 nm region with the sum peaked at ~274 nm. The two absorption bands of each conformer exhibit some overlap and appear to merge together for the *syn-trans* conformer.

Potential energy curves (unrelaxed) along the O—O dissociation coordinate are also evaluated using the CASPT2(12,10)/AVDZ level of theory by elongating the O—O bond, while keeping other degrees of freedom fixed at the ground state optimized geometry for the *syn-trans* conformer of MVK-oxide. The resultant diabatic singlet potential curves (unrelaxed) are shown in Fig. 3. Vertical excitation of the *syn-trans* conformer to the $1^1\pi\pi^*$ state at 3.54 eV (351 nm) is predicted to access a repulsive region of the excited state potential, which leads to a conical intersection with a repulsive potential (estimated at ~2.78 eV; 446 nm) and results in dissociation to *trans*-MVK $X\,^1A' + O\,^1D$ products. (Note that more extensive calculations, which are beyond the scope of the present work, are required to map the conical intersection region accurately.) A similar dissociation pathway has previously been mapped out for CH_2OO following electronic excitation to an analogous $1^1\pi\pi^*$ state.[30,36,38] The vertical transition and simulated absorption spectrum for *syn-trans*-MVK-oxide are also shown (Fig. 3). The zero-point corrected energy required for spin-allowed dissociation of the *syn-trans* conformer of MVK-oxide to *trans*-MVK $X\,^1A' + O\,^1D$ is computed to be 2.25 eV (18180 cm^{-1}, 550 nm) based on a relaxed optimization at large O—O separation. The dissociation energy predicted for MVK-oxide to its lowest spin-allowed asymptote is similar to that determined previously for $CH_2OO\ X\,^1A'$ to $H_2CO\ X\,^1A_1 + O\,^1D$ products.[40,41,61]

Zero-point corrected dissociation energies for other MVK-oxide conformers (Table S3) are evaluated by taking into account their relative ground state stabilities (Table S1) and the small energy splitting (84 cm^{-1}; B2PLYP-D3/VTZ) predicted between the *cis* and *trans* conformers of the MVK product.

Previously, the vertical and adiabatic ionization energies for several possible isomers of MVK-oxide were also calculated at the CCSD(T)-F12/CBS(TZ-F12,QZ-F12)//B2PLYP-D3/VTZ level of theory (Table S1, Ref. 25). In this work, the vertical electronic transitions and oscillator strengths for these possible isomers of MVK-oxide are also evaluated at the CASPT2(12,10)/AVDZ level of theory and are given in Table S4. Potential isomers of MVK-oxide that may be generated and their detection by photoionization and/or UV-vis spectroscopy are considered in Sec. V.

III. EXPERIMENTAL METHODS

A new synthetic route is used to generate MVK-oxide starting from a (Z/E)-1,3-diiodobut-2-ene precursor as described previously.[25] As shown in Scheme S1, photolysis of 1,3-diiodobut-2ene at 248 nm results in preferential dissociation of the weaker allylic $C_{(1)}I$ bond due to resonance stabilization of the resultant allylic monoiodoalkene radical product Int(1). Although the radical center is initially formed at the $C_{(1)}$ carbon, delocalization will lead to the preferred radical site on the $C_{(3)}$ carbon. Subsequent addition of O_2 is barrierless at the $C_{(3)}$ carbon site of Int(1), transiently forming an energized iodoalkene peroxy radical Int(2) that can readily rotate about the C—C and C—O bonds, prior to dissociation to produce MVK-oxide. The O_2 reaction step is similar to that leading to other Criegee intermediates from their corresponding geminal diiodo precursors.

The generation of Criegee intermediates in a pulsed supersonic expansion in this laboratory has been described previously.[27–29] In the present study, the diiodoalkene precursor is heated (60 °C) in a pulsed solenoid valve (Parker-Hannifin General Valve) with a Peltier thermoelectric heating module (Laird Technologies, PC4). The temperature is monitored with a thermocouple (Cole-Parmer, Type K digital thermometer). The precursor is seeded in a 20% O_2/Ar carrier gas (12 psig) and pulsed through a nozzle (1 mm orifice) into a quartz capillary tube reactor (1 mm ID; ~25 mm length). The precursor is photolyzed along the length of the capillary tube using the cylindrically focused 248 nm output (25 mJ pulse^{-1}) of a KrF excimer laser (Coherent, Compex 102, 10 Hz), which induces C—I bond dissociation. Subsequent reaction of the resonance-stabilized monoiodoalkene radical with O_2 produces the MVK-oxide intermediate. MVK-oxide is collisionally stabilized in the capillary tube and cooled in the ensuing supersonic expansion to a rotational temperature of ~10 K.

For photoionization measurements, the gas mixture travels ~4 cm downstream into a collision free region. Here, it is crossed by focused VUV radiation (118 nm) that is generated by frequency tripling the third harmonic output (~35 mJ/pulse) of a Nd:YAG laser (Continuum Powerlite 9010) in a phase matched Xe:Ar gas mixture. Single photon excitation
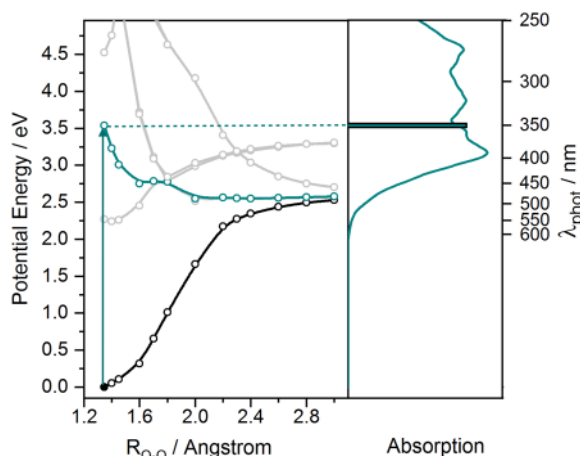

FIG. 3. (Left panel) Potential energy curves (unrelaxed) computed along the O—O bond dissociation coordinate for the lowest seven singlet states of the *syn-trans* conformer of MVK-oxide. The lower potentials curves (including black and cyan curves) lead to *trans*-MVK $X\,^1A' + O\,^1D$ products, while the higher potential curves dissociate to *trans*-MVK $a\,^3A'' + O\,^3P$ products. Calculations are performed at CASPT2(12,10)/AVDZ level of theory. Vertical transition (arrow) from the ground S_0 electronic state (black curve) to the $1^1\pi\pi^*$ state (cyan curve) is predicted at 3.54 eV (351 nm). (Right panel) Computed vertical electronic transition (bar) and associated absorption spectrum (curve) for $\pi^* \leftarrow \pi$ transitions based on a harmonic-oscillator Wigner distribution for the S_0 state.

with 118 nm (10.5 eV) radiation results in ionization. The m/z = 86 mass channel is monitored using a Wiley McLaren linear TOF mass spectrometer (Jordan).

UV-vis radiation is generated using a broadly tunable β-barium borate-optical parametric oscillator (BBO-OPO) source (EKSPLA 342NT, pulse width of 3-5 ns, <5 cm^{-1} linewidth). The signal output is utilized in the 410-500 nm region and sum frequency generation (SFG) of the frequency-doubled signal output + 1064 nm Nd:YAG fundamental is utilized in the 305-409 nm region. The wavelength (vacuum) of the BBO-OPO output is calibrated using a high resolution wavemeter (Coherent WaveMaster). The UV-vis OPO power is carefully adjusted and measured with a power meter (Gentec TPM3/300).

UV-vis depletion measurements of MVK-oxide are performed by introducing UV-vis radiation ~50 ns prior to VUV photoionization, as described previously.[27–29] The counter-propagating UV-vis radiation is focused (30 cm focal length) and spatially overlapped with the VUV radiation in the ionization region of the TOF. The VUV laser is operated at 10 Hz, while the BBO-OPO is run at 5 Hz to obtain the UV-vis induced fractional depletion [(UV-vis off − UV-vis on)/(UV-vis off)] or percentage depletion (when multiplied by 100%) of the photoionization signal on alternating shots.

In addition, velocity-map images (VMI) of the O ^{1}D products are obtained following UV-vis excitation of MVK-oxide, as described previously for other Criegee intermediates.[37,40,41,61] Again, UV-vis excitation is generated from the BBO-OPO source (~2 mJ/pulse) and focused (70 cm focal length) in the interaction region. The O ^{1}D dissociation products are ionized via 2 + 1 resonance enhanced multiphoton ionization (REMPI) at 205.47 nm,[62] which is generated by frequency tripling of the output of a Nd:YAG (Continuum Powerlite 8010) pumped dye laser (Continuum, ND6000, Rh 610) and scanned over the O-atom Doppler profile (±0.4 cm^{-1}). The counterpropagating UV probe laser is focused (40 cm focal length) into the interaction region, where it is spatially overlapped with the UV-vis pump OPO at a time delay of 50 ns. The UV-vis pump and UV probe polarizations are aligned and both oriented parallel to the microchannel plate (MCP) detection plane. The ions are velocity focused onto the spatially sensitive MCP detector, which is gated for the O$^+$ mass channel (m/z = 16). The central region of the detector is protected using a beam block, which prevents ions with low translational energy (<150 cm^{-1}) from striking the MCP plate.[40,41] The pancaked image is then analyzed using the pBASEX inversion method to extract the angular and velocity distributions of the O ^{1}D products.[63] An active background subtraction scheme is implemented by running the UV-vis OPO at 5 Hz, while the REMPI laser is operated at 10 Hz. The subtracted background originates from 205 nm excitation of the IO by-product[64] and the $2\,^1\pi\pi^*$ transition of MVK-oxide, both of which yield O ^{1}D products.

IV. RESULTS

The MVK-oxide Criegee intermediate was initially detected by photoionization using 10.5 eV (118 nm) VUV radiation on the m/z = 86 mass channel of the TOF mass spectrometer as shown in Fig. 4. The VUV photoionization signal at m/z = 86 is observed upon excimer photolysis of the diiodo alkene precursor in the reactor tube with O_2 in the carrier gas mixture. The 10.5 eV photoionization energy exceeds the computed ionization energy of 8.5-9.0 eV (Table I) for the four MVK-oxide conformers; other isomers that may be generated in the source and ionized at 10.5 eV will also be considered in the discussion. Here, we assume that the four MVK-oxide conformers are generated with similar yield, have similar ionization efficiencies at 10.5 eV, and contribute equally to the photoionization signal at m/z = 86. Further studies will be needed to determine the MVK-oxide conformer distribution, for example, by conformer specific unimolecular[25] and/or bimolecular[33] reaction rates. Recently, MVK-oxide was characterized utilizing IR action spectroscopy, in which characteristic IR transitions of MVK-oxide were identified at ~6000 cm^{-1} and detected through the resultant appearance of OH products.[25] The present study focuses on characterizing MVK-oxide through the very strong $\pi^* \leftarrow \pi$ electronic transitions (Fig. 2, Table I) predicted for its four conformers in the UV-vis region.

Here, we demonstrate that UV-vis excitation resonant with the first $\pi^* \leftarrow \pi$ electronic transition depletes the ground-state population of one or more of the four MVK-oxide conformers. The ground state depletion is readily detected after a short time delay (Δt ~ 50 ns) using VUV photoionization as a reduced signal at m/z = 86. Figure 4 shows a representative example, in which UV excitation at 390 nm (0.7 mJ/pulse) induces a ~20% decrease in the VUV photoionization signal at m/z = 86. The signal [(UV off – UV on)/UV off] × 100% yields a ~20% depletion. The depletion increases with UV power, as shown in Fig. 5, reaching a maximum depletion of ~25%
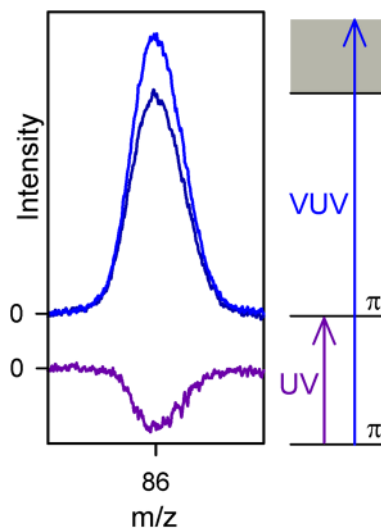

FIG. 4. Mass spectra (m/z = 86) arising from photoionization of MVK-oxide with VUV radiation at 118 nm (10.5 eV). The top trace (blue) shows the photoionization signal. The middle trace (dark blue) shows the significant reduction (~20%) in the photoionization signal upon focused UV excitation at 390 nm (0.7 mJ/pulse) on the first $\pi^* \leftarrow \pi$ transition, which results in ground state depletion. The lower trace (purple) shows the depletion signal (UV on–UV off). Also shown is a schematic energy level diagram indicating the π and π* states and ionization limit (shaded) for the MVK-oxide Criegee intermediate.
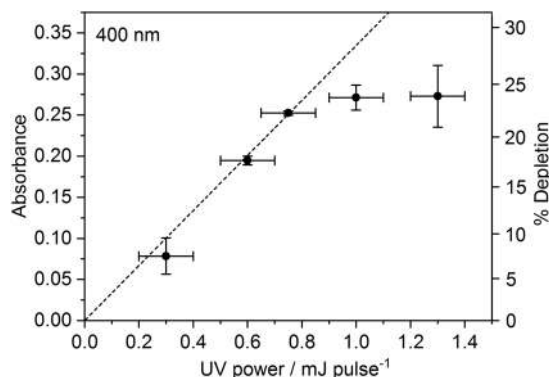
FIG. 5. Percentage depletion of the m/z = 86 (MVK-oxide$^+$) ion signal $(N_0 - N)/N_0 * 100\%$ with ground state abundances N_0 before and N after irradiation as a function of the OPO power at 400 nm. The error bars represent the standard deviation ($\pm 1\sigma$) derived from repeated measurements. The corresponding absorbance, $-\ln(N/N_0)$, changes linearly (dashed line) at excitation energies up to 0.8 mJ/pulse indicating a one-photon process. No further depletion is observed at higher OPO powers. This suggests that more than one MVK-oxide conformer, isomer, or dissociative ionization fragment may contribute to the photoionization signal at m/z = 86, but does not strongly absorb and/or dissociate upon UV-vis excitation.

at 400 nm. A minimum depletion of 2-3% can be reliably measured at the current signal levels. The magnitude of the depletion can be expressed as $(N_0 - N)/N_0$ with ground state abundances N_0 before and N after UV irradiation. The corresponding absorbance, $-\ln(N/N_0)$, scales linearly with OPO power up to ~0.8 mJ/pulse. The linear dependence indicates a one-photon absorption process. The magnitude of the depletion is unchanged beyond 25% at higher power. This suggests that more than one MVK-oxide conformer, isomer, or possibly a dissociative ionization fragment may contribute to the m/z = 86 photoionization signal. Such additional species do not appear to strongly absorb and/or rapidly dissociate upon UV-vis excitation. Nevertheless, the large magnitude of the depletion and associated absorbance are indicative of a strong electronic transition for MVK-oxide, as observed previously for other carbonyl oxide species.[27–29] UV-vis excitation also results in a small increase in the m/z = 70 mass, likely due to photoionization of MVK.

The UV-vis radiation from the BBO-OPO is scanned across the UV-vis region from 305 to 480 nm to obtain the electronic spectrum of MVK-oxide by means of the UV-vis induced depletion of the associated VUV photoionization signal. The resultant UV-vis spectrum shown in Fig. 6 is recorded in 1 nm steps and normalized to OPO power, which is maintained at less than 1 mJ/pulse throughout the entire spectral region (specifically, 0.5-0.7 mJ/pulse in the central 360-420 nm region). The data points are averages of repeated measurements with $\pm 1\sigma$ uncertainty indicated by the shaded region; the smooth line is a polynomial fit through the data. The broad and unstructured experimental MVK-oxide spectrum exhibits an asymmetric shape with its peak at 388 nm. The experimental spectrum decreases to half maximum at 345 nm on the shorter wavelength side and falls off sharply to half maximum at 412 nm on the longer wavelength side. The spectrum drops to a minimal observable level at ca. 450 nm and terminates by ~475 nm. The unusual shape of the experimental spectrum originates in part from overlapping absorption
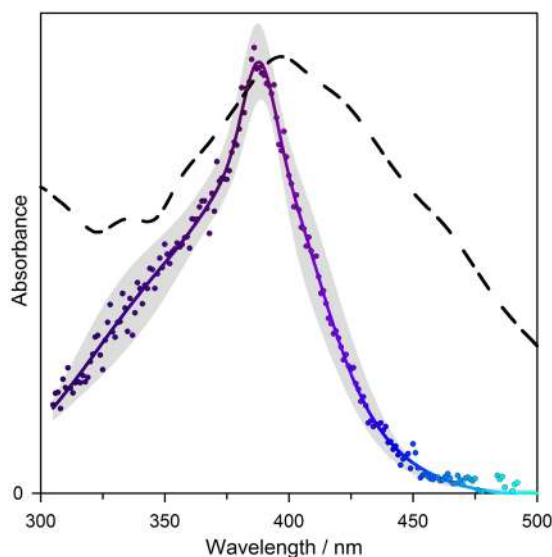

FIG. 6. Experimental UV-vis spectrum of MVK-oxide from 305 to 480 nm derived from depletion of the photoionization signal on the m/z = 86 mass channel. The corresponding absorbance (points) is plotted after normalizing for OPO power. The solid line represents a polynomial fit through the experimental data, while the shaded area indicates the $\pm 1\sigma$ uncertainty. The overall MVK-oxide electronic absorption spectrum (dashed line) computed for the four conformers is shown for comparison.

spectra of the four conformers of MVK-oxide as predicted theoretically (Fig. 2). The peak of the experimental spectrum agrees well with the predicted peak at 397 nm of the cumulative absorption spectrum involving the first optically bright $\pi^* \leftarrow \pi$ ($1^1\pi\pi^*$) transition computed theoretically. The experimental spectrum does not terminate at 305 nm and actually increases again to shorter wavelength (not shown), which is likely due to excitation to the $2^1\pi\pi^*$ state and will be presented in a future publication. However, the experimental spectrum falls off far more sharply on the long wavelength side than predicted theoretically in the cumulative absorption spectrum. We consider possible reasons for the discrepancy between the experiment and theory in the long wavelength falloff region in Sec. V.

We can roughly estimate the absorption cross section $\sigma(\lambda)$ of MVK-oxide at 388 nm by dividing the absorbance by the photon flux Φ (mJ/cm^2) of the focused UV beam in the interaction region. At an UV power of 0.7 mJ/pulse and an approximate area of ~0.05 cm^2, corresponding to a photon flux of 14 mJ/cm^2, we estimate a peak absorption cross section on the order of 10^{-17} cm^2 molec^{-1}. This estimate is in good accord with absorption cross sections obtained previously for prototypical Criegee intermediates at their peak wavelengths.[27–29,34,35] However, this rough estimate does not take into account that the four conformers of MVK-oxide may make different contributions (based on conformer population, photoionization efficiency at 10.5 eV, and/or absorption cross section at 390 nm) to the UV-induced depletion at 390 nm. In addition, other species (see Sec. V) may contribute to the photoionization signal at m/z = 86, but not result in a UV-induced depletion at 390 nm, thereby reducing the apparent absorbance of MVK-oxide. Finally, the estimated cross section does not take into account the spatial profile of the UV-vis OPO beam.

Additional pump-probe experiments are carried out using UV-vis excitation of MVK-oxide and 2 + 1 REMPI detection of O ^{1}D products. The O$^+$ ions are detected using velocity map imaging, which reveals the velocity and angular distribution of the fragments. O ^{1}D VMI images are obtained at discrete wavelengths from 234 to 420 nm, although here we focus exclusively on the images obtained at 390 and 420 nm that are shown in Fig. 7; VMI results at other wavelengths will be presented in a future publication. The O ^{1}D signal drops off rapidly at longer excitation wavelengths with only a very weak signal at ca. 430 nm (insufficient for an image) and no detectable signal beyond 440 nm. The lack of observable O ^{1}D products beyond 440 nm (less than 2.8 eV) is consistent with long wavelength falloff of the depletion spectrum. Dissociation of MVK-oxide to MVK X ^{1}A′ + O ^{1}D products is theoretically predicted to be accessible at much lower energies (2.25 eV product asymptote for *syn-trans* conformer), corresponding to wavelengths beyond 550 nm (see Table S3).

As evident in Fig. 7, the VMI images at 390 and 420 nm show distinctive angular distributions indicative of rapid dissociation to O ^{1}D products on a time scale faster than the MVK-oxide rotational period (~100 ps). The implication is that electronic excitation of MVK-oxide at λ ≤ 420 nm accesses repulsive regions of the $1^1\pi\pi^*$ potential energy curve (Fig. 3), which results in prompt dissociation to MVK X ^{1}A′ + O ^{1}D products. The resultant total kinetic energy release (TKER) distributions are broad and structureless. Remarkably, the TKER distributions have similar average translational energies of ~2100 cm^{-1}, breadths of ~1750 cm^{-1}, and extend out to ~4000 cm^{-1}. The similar TKER distributions are

notable given that far more energy (1830 cm^{-1}) is available to products upon 390 nm vs. 420 nm excitation of MVK-oxide. The similar kinetic energy release suggests the possibility of a barrier along the dissociation pathway to products with the kinetic energy release reflecting the barrier height.[65] In this case, the barrier would be associated with the conical intersection (estimated at ~2.78 eV) leading to products, as discussed in Sec. V A. A comprehensive analysis of the VMI images yields parameters for the angular anisotropy and total kinetic energy release given in Table S5, which will be detailed in a future publication. The theoretically predicted dissociation energy (zero-point corrected) for the *syn-trans* conformer of MVK-oxide to *trans*-MVK X ^{1}A′ + O ^{1}D products is 2.25 eV (Table S3), from which we estimate a much greater energy available (E_{avl}) to products of 7460 and 5360 cm^{-1} (Table S5) at 390 and 420 nm, respectively, than observed experimentally.

V. DISCUSSION

A. Comparison of experimental and theoretical MVK-oxide UV-vis spectra

The experimental UV-vis spectrum for MVK-oxide, recorded by depletion of the photoionization signal at m/z = 86, peaks at 388 nm and compares favorably with the peak of the computed cumulative absorption spectrum for MVK-oxide on the first $\pi^* \leftarrow \pi$ transition at 397 nm. The theoretical prediction assumes equal population of the four conformers of MVK-oxide, each of which has its own broad, but distinctive absorption spectrum. Both the experiment and theory demonstrate that the MVK-oxide spectrum peaks at significantly longer wavelength than previously characterized Criegee intermediates (CH$_2$OO at 335 nm;[27,31,32] *syn*-CH$_3$CHOO,[28,33,34] (CH$_3$)$_2$COO and CH$_3$CH$_2$CHOO at ~320 nm;[29,35] and *anti*-CH$_3$CHOO at ~360 nm).[33] The first $\pi^* \leftarrow \pi$ transition of MVK-oxide is shifted to longer wavelength as a result of extended conjugation spanning across the carbonyl oxide and vinyl groups.[53]

The experimental and computed spectra for MVK-oxide (Fig. 6) differ in the long wavelength region beyond the peak of the cumulative theoretical spectrum predicted using CASPT2 (Fig. 2). From the theoretical perspective, it is possible that the harmonic-oscillator Wigner distribution of initial MVK-oxide geometries oversample distorted (higher energy) ground state configurations that would require lower excitation energies to reach the excited $1^1\pi\pi^*$ state. (There may also be limitations in the CASPT2 calculations at these geometries.) This could extend the theoretically predicted absorption spectrum to longer wavelengths. Another possible explanation might be that some MVK-oxide conformers (e.g., *anti-trans* with predicted maximum at 440 nm) are significantly less populated than other conformers under our experimental conditions. Further experiments examining conformer-specific unimolecular and/or bimolecular reaction will be required to determine the conformer distribution. However, we note that a recent IR experimental study provides evidence that both *syn* and *anti* conformers of MVK-oxide are generated from the diiodoalkene precursor and observed under similar conditions.[25]
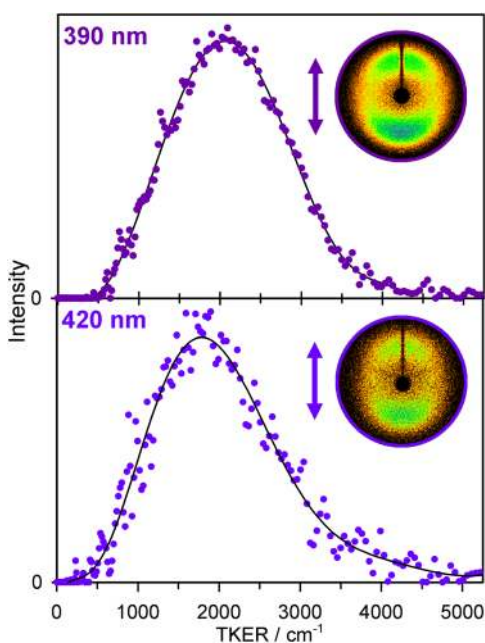

FIG. 7. Total kinetic energy release (TKER) distributions (points) and polynomial fits (line) for the O(^{1}D) + MVK products obtained by velocity map imaging following UV-vis excitation of MVK-oxide at 390 nm (upper panel) and 420 nm (lower panel). Corresponding raw images of the O(^{1}D) photoproducts are shown as insets. The blue double-sided arrows represent the polarization of the UV-vis OPO (parallel to the detector plane).

The UV-vis spectrum of MVK-oxide obtained by the depletion method will be equivalent to a standard absorption measurement if MVK-oxide promoted to the $1^1\pi\pi^*$ excited state undergoes prompt dynamics that preclude ionization and detection at m/z = 86. Rapid dissociation ($\leq$100 ps) to MVK + O ^{1}D is demonstrated in the present study by detection of an anisotropic distribution of O ^{1}D products in VMI images at $\lambda \leq 420$ nm. Theoretical calculations also indicate that UV-vis excitation of MVK-oxide at $\lambda \leq 420$ nm accesses a repulsive region of the $1^1\pi\pi^*$ potential (Fig. 3). This leads to a conical intersection with strong coupling to repulsive singlet potential(s) and results in dissociation to MVK X ^{1}A′ + O ^{1}D products. Electronic excitation of MVK-oxide at energies above the conical intersection region is expected to result in prompt O—O bond dissociation. The energy release associated with the effective barrier to products ($\sim$4000 cm^{-1}) is expected to flow primarily into kinetic energy[65] and is qualitatively consistent with the range of TKER observed experimentally. At lower energies, an effective barrier associated with the conical intersection would preclude dissociation except possibly through O-atom tunnelling on a much slower time scale.[66]

Theoretical calculations predict that the long wavelength region of the MVK-oxide absorption spectrum extends beyond the conical intersection region ($\sim$450 nm) and the MVK X ^{1}A′ + O ^{1}D product asymptote ($\sim$550 nm, Table S3), corresponding to energies below the conical intersection region ($\sim$2.78 eV) and product asymptote (2.25 eV for the syn-trans conformer, Table S3). In this long wavelength region, electronically excited MVK-oxide may not dissociate and could decay by a different mechanism. Alternative decay pathways such as internal conversion or fluorescence to the ground electronic state are expected to be fast compared to the 50 ns delay prior to VUV photoionization. In particular, internal conversion would result in vibrationally excited MVK-oxide that can rapidly undergo various unimolecular decay processes and lead to fragmentation (see Sec. V B and Ref. 25). As a result, repopulation of the ground electronic state of MVK-oxide and the subsequent photoionization that could reduce and/or eliminate the depletion in the photoionization signal at long wavelengths ($\lambda \geq 450$ nm) seem to be an unlikely scenario.[31] Nevertheless, the present depletion measurements will be compared with future direct absorption measurements and together will provide a further test of the calculated absorption spectrum.

B. Electronic transitions of other possible isomers

In a recent study, this laboratory demonstrated that vibrational activation of syn-MVK-oxide with two quanta of CH stretch induces unimolecular decay to OH products,[25] as found for other syn-methyl substituted Criegee intermediates.[7–9,67–69] Infrared spectral features and associated unimolecular decay rates were obtained with detection of the OH products. Unimolecular decay of syn-MVK-oxide proceeds via a 1,4 H-atom transfer mechanism though a transition state (TS) to 2-hydroperoxybuta-1,3-diene ((CH$_2$=CH)(CH$_2$)COOH, HPBD) with subsequent O—O bond fission to OH + oxybutadiene ((CH$_2$=CH)(CH$_2$)CO, OBD) radicals as depicted in Scheme 2.
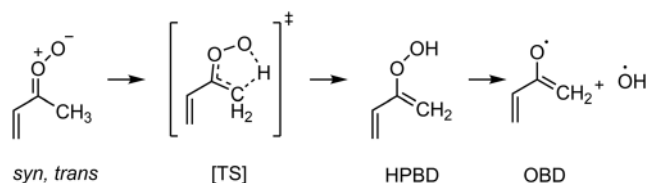

SCHEME 2. 1,4 H-atom transfer pathway for unimolecular decay of syn-MVK-oxide Criegee intermediate via HPBD to OH radical.

Master equation modeling showed that unimolecular decay of syn-MVK-oxide is also expected to occur under atmospheric conditions with a rate of $\sim$33 s^{-1} (298 K, 1 atm). Here, we consider whether the HPBD intermediate, e.g., formed in the capillary reactor tube, could contribute to the UV-vis spectrum attributed to MVK-oxide (Fig. 6). While HPBD could be ionized at 10.5 eV (Table S1, Ref. 25), the present CASPT2(12,10)/AVDZ calculations indicate that neither trans- nor cis-HPBD are expected to absorb in the 300-500 nm region (Table S4); HPBD's electronic transitions are predicted to lie further to the UV (below 220 nm). An alternative unimolecular reaction pathway of HPBD was identified theoretically to lead to 1-hydroxybut-3-en-2-one (CH$_2$CHC(O)CH$_2$OH, HB).[25] HB may be formed via a roaming induced isomerization at long range involving addition of OH to the CH$_2$ group of OBD. Again, the HB roaming product may be ionized at 10.5 eV,[25] but HB is only predicted to absorb strongly below 205 nm (Table S4).

For anti-MVK-oxide, a recent theoretical examination of unimolecular decay pathways indicated that isomerization to 5-methyl-3H-1,2-dioxole (cyc-CH$_2$OOC(CH$_3$)CH, dioxole) is the most likely initial step to products. anti-MVK-oxide is predicted to undergo an electrocyclic ring-closing reaction via a low barrier to form the 5-membered ring of dioxole, as shown in Scheme 3.

Master equation modeling suggests a relatively fast thermal unimolecular reaction rate to dioxole of 2140 s^{-1} (298 K, 1 atm)[25] and potentially a high yield (36%-42%).[19] Again, if dioxole is formed and stabilized, e.g., in the reactor tube, it could be ionized at 10.5 eV, but its first strong electronic transition is predicted at 211 nm. Initially formed dioxole would likely be internally excited and could decay by O—O bond fission to form a diradical, which can rearrange to a number of dicarbonyl and enol compounds.[19] Representative examples of product compounds, e.g., 3-oxobutanal (CH(O)CH$_2$C(O)CH$_3$, β-dicarbonyl) and 3-hydroxybut-2-enal (CH(O)CHCH(OH)CH$_3$, enol), could again be ionized at 10.5 eV, but are only predicted to have strong electronic transitions below 300 nm (Table S4).

While there are many possible isomers of MVK-oxide that may be ionized at 10.5 eV (Table S1, Ref. 25), we have not identified a plausible isomer that is also predicted to have strong electronic transitions in the 300-500 nm region. On the other hand, the present CASPT2(12,10)/AVDZ calculations for each of the four conformers of MVK-oxide indicate a strong $\pi^* \leftarrow \pi$ transition with vertical excitation in the 350-400 nm region and simulated absorption spectra spanning from 325 to 600 nm. The experimental spectrum peaks at 388 nm, which is in very good accord with the cumulative calculated absorption profile with its maximum 397 nm.
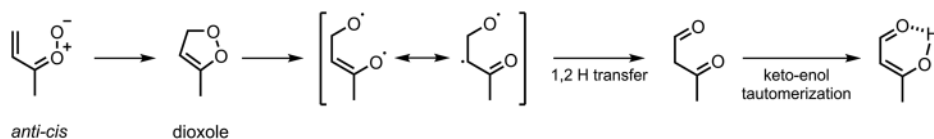
SCHEME 3. Mechanism from *anti*-MVK-oxide unimolecular decay via dioxole intermediate and other unimolecular rearrangements.

VI. CONCLUSIONS

The four-carbon unsaturated Criegee intermediate MVK-oxide, produced in nature by isoprene ozonolysis, has been generated in the laboratory by an alternative synthetic route involving a resonantly stabilized iodoalkene radical. The UV-vis spectrum of MVK-oxide on its first $\pi^* \leftarrow \pi$ electronic transition has been recorded by the UV-vis induced depletion of the VUV (10.5 eV) photoionization signal at m/z = 86. The strong UV-vis induced depletion (up to 25%) of one or more of the four MVK-oxide conformers peaks at 388 nm in a one-photon absorption process. The broad and unstructured experimental spectrum recorded with a continuously tunable BBO-OPO spans from at least 300 to 430 nm. Additional velocity map imaging experiments demonstrate that electronic excitation of MVK-oxide in this spectral region results in rapid dissociation ($\leq$100 ps) to O ^{1}D products.

Complementary theoretical calculations predict vertical transition energies and large oscillator strengths for transitions of MVK-oxide to the $1^1\pi\pi^*$ and $2^1\pi\pi^*$ states in the 3.1-3.6 eV (350-400 nm) and 4.5-5.5 eV (220-280 nm) regions, respectively. These two optically bright transitions are nominally associated with the carbonyl oxide and vinyl groups, but the calculations demonstrate that the π and π^* orbitals of MVK-oxide are delocalized across the entire molecule. The UV-vis absorption profiles of the MVK-oxide conformers are computed using a Wigner distribution of initial configurations. The resultant cumulative absorption spectrum for the first $\pi^* \leftarrow \pi$ transition, based on equal population of the four conformers, is computed to peak at 397 nm and extend to long wavelengths beyond the MVK X ^{1}A′ + O ^{1}D product asymptote at ~550 nm (~2.25 eV for *syn-trans* conformer).

Electronic excitation of MVK-oxide to the $1^1\pi\pi^*$ state accesses a repulsive region of the excited state potential energy surface, leading to a conical intersection (estimated at ~2.78 eV; 446 nm for *syn-trans* conformer) with a repulsive potential that results in dissociation. At excitation energies above the conical intersection region, the resultant dissociation is expected to be prompt to MVK X ^{1}A′ + O ^{1}D products. At lower energies, the conical intersection may act as an effective barrier to dissociation. As a result, comparison of the present depletion measurements with future direct absorption measurements are planned to further evaluate the predicted theoretical spectrum. Finally, electronic transitions of several possible isomers of MVK-oxide are predicted to absorb at much shorter wavelength than the first strong $\pi^* \leftarrow \pi$ transition identified for the four-carbon unsaturated MVK-oxide Criegee intermediate in this study.

The strong $\pi^* \leftarrow \pi$ electronic transition of MVK-oxide is distinctive from previously studied Criegee intermediates due to extended conjugation across the carbonyl oxide and vinyl groups. Identification of the UV-vis spectrum of MVK-oxide is expected to enable future studies of its photochemistry,

unimolecular decay processes, and bimolecular reactions with key atmospheric species. In turn, these ongoing and future studies may help unravel the contributions of the four conformers of MVK-oxide to the UV-vis spectrum presented here.

SUPPLEMENTARY MATERIAL

See supplementary material for the precursor synthesis method, additional figures and tables providing details on the electronic structure calculations of MVK-oxide and several possible isomers, and parameters extracted from experimental velocity map imaging experiments.

[1]K. Sindelarova, C. Granier, I. Bouarar, A. Guenther, S. Tilmes, T. Stavrakou, J. F. Müller, U. Kuhn, P. Stefani, and W. Knorr, Atmos. Chem. Phys. **14**, 9317–9341 (2014).
[2]R. Atkinson and J. Arey, Acc. Chem. Res. **31**, 574–583 (1998).
[3]R. Atkinson and J. Arey, Chem. Rev. **103**, 4605–4638 (2003).
[4]R. Atkinson and J. Arey, Atmos. Environ. **37**, 197–219 (2003).
[5]D. Johnson and G. Marston, Chem. Soc. Rev. **37**, 699–716 (2008).
[6]G. T. Drozd, T. Kurten, N. M. Donahue, and M. I. Lester, J. Phys. Chem. A **121**, 6036–6045 (2017).
[7]Y. Fang, V. P. Barber, S. J. Klippenstein, A. B. McCoy, and M. I. Lester, J. Chem. Phys. **146**, 134307 (2017).
[8]Y. Fang, F. Liu, V. P. Barber, S. J. Klippenstein, A. B. McCoy, and M. I. Lester, J. Chem. Phys. **145**, 234308 (2016).
[9]Y. Fang, F. Liu, V. P. Barber, S. J. Klippenstein, A. B. McCoy, and M. I. Lester, J. Chem. Phys. **144**, 061102 (2016).
[10]R. L. Mauldin III, T. Berndt, M. Sipilä, P. Paasonen, T. Petäjä, S. Kim, T. Kurtén, F. Stratmann, V. M. Kerminen, and M. Kulmala, Nature **488**, 193–196 (2012).
[11]J. P. Hakala and N. M. Donahue, J. Phys. Chem. A **120**, 2173–2178 (2016).
[12]W. Chao, J.-T. Hsieh, C.-H. Chang, and J. J.-M. Lin, Science **347**, 751–754 (2015).
[13]H.-L. Huang, W. Chao, and J. J.-M. Lin, Proc. Natl. Acad. Sci. U. S. A. **112**, 10857–10862 (2015).

[14]L.-C. Lin, H.-T. Chang, C.-H. Chang, W. Chao, M. C. Smith, C.-H. Chang, J. J.-M. Lin, and K. Takahashi, Phys. Chem. Chem. Phys. **18**, 4557–4568 (2016).

[15]T. R. Lewis, M. A. Blitz, D. E. Heard, and P. W. Seakins, Phys. Chem. Chem. Phys. **17**, 4859–4863 (2015).

[16]J. H. Kroll and J. H. Seinfeld, Atmos. Environ. **42**, 3593–3624 (2008).

[17]T. F. Mentel, M. Springer, M. Ehn, E. Kleist, I. Pullinen, T. Kurtén, M. Rissanen, A. Wahner, and J. Wildt, Atmos. Chem. Phys. **15**, 6745–6765 (2015).

[18]R. Gutbrod, E. Kraka, R. N. Schindler, and D. Cremer, J. Am. Chem. Soc. **119**, 7330–7342 (1997).

[19]K. T. Kuwata, L. C. Valin, and A. D. Converse, J. Phys. Chem. A **109**, 10710–10725 (2005).

[20]K. T. Kuwata and L. C. Valin, Chem. Phys. Lett. **451**, 186–191 (2008).

[21]T. B. Nguyen, G. S. Tyndall, J. D. Crounse, A. P. Teng, K. H. Bates, R. H. Schwantes, M. M. Coggon, L. Zhang, P. Feiner, D. O. Milller, K. M. Skog, J. C. Rivera-Rios, M. Dorris, K. F. Olson, A. Koss, R. J. Wild, S. S. Brown, A. H. Goldstein, J. A. de Gouw, W. H. Brune, F. N. Keutsch, J. H. Seinfeld, and P. O. Wennberg, Phys. Chem. Chem. Phys. **18**, 10241–10254 (2016).

[22]S. M. Aschmann and R. Atkinson, Environ. Sci. Technol. **28**, 1539–1542 (1994).

[23]C. A. Taatjes, O. Welz, A. J. Eskola, J. D. Savee, A. M. Scheer, D. E. Shallcross, B. Rotavera, E. P. F. Lee, J. M. Dyke, D. K. W. Mok, D. L. Osborn, and C. J. Percival, Science **340**, 177–180 (2013).

[24]O. Welz, J. D. Savee, D. L. Osborn, S. S. Vasu, C. J. Percival, D. E. Shallcross, and C. A. Taatjes, Science **335**, 204–207 (2012).

[25]V. P. Barber, S. Pandit, A. M. Green, N. Trongsiriwat, P. J. Walsh, S. R. Klippenstein, and M. I. Lester, J. Am. Chem. Soc. **140**, 10866–10880 (2018).

[26]P. Aplincourt, E. Henon, and F. Bohr, Chem. Phys. **285**, 221–231 (2002).

[27]J. M. Beames, F. Liu, L. Lu, and M. I. Lester, J. Am. Chem. Soc. **134**, 20045–20048 (2012).

[28]J. M. Beames, F. Liu, L. Lu, and M. I. Lester, J. Chem. Phys. **138**, 244307 (2013).

[29]F. Liu, J. M. Beames, A. M. Green, and M. I. Lester, J. Phys. Chem. A **118**, 2298–2306 (2014).

[30]K. Samanta, J. M. Beames, M. I. Lester, and J. E. Subotnik, J. Chem. Phys. **141**, 134303 (2014).

[31]L. Sheps, J. Phys. Chem. Lett. **4**, 4201–4205 (2013).

[32]W.-L. Ting, Y.-H. Chen, W. Chao, M. C. Smith, and J. J.-M. Lin, Phys. Chem. Chem. Phys. **16**, 10438–10443 (2014).

[33]L. Sheps, A. M. Scully, and K. Au, Phys. Chem. Chem. Phys. **16**, 26701–26706 (2014).

[34]M. C. Smith, W. L. Ting, C. H. Chang, K. Takahashi, K. A. Boering, and J. J. Lin, J. Chem. Phys. **141**, 074302 (2014).

[35]Y.-P. Chang, C.-H. Chang, K. Takahashi, and J. J.-M. Lin, Chem. Phys. Lett. **653**, 155–160 (2016).

[36]R. Dawes, B. Jiang, and H. Guo, J. Am. Chem. Soc. **137**, 50–53 (2015).

[37]M. F. Vansco, H. Li, and M. I. Lester, J. Chem. Phys. **147**, 013907 (2017).

[38]Q. Meng and H. D. Meyer, J. Chem. Phys. **141**, 124309 (2014).

[39]R. Chhantyal-Pun, A. Davey, D. E. Shallcross, C. J. Percival, and A. J. Orr-Ewing, Phys. Chem. Chem. Phys. **17**, 3617–3626 (2015).

[40]H. Li, Y. Fang, J. M. Beames, and M. I. Lester, J. Chem. Phys. **142**, 214312 (2015).

[41]H. Li, Y. Fang, N. M. Kidwell, J. M. Beames, and M. I. Lester, J. Phys. Chem. A **119**, 8328–8337 (2015).

[42]L. Goerigk and S. Grimme, J. Chem. Theory Comput. **7**, 291–309 (2011).

[43]S. Grimme, S. Ehrlich, and L. Goerigk, J. Comput. Chem. **32**, 1456–1465 (2011).

[44]R. A. Kendall, T. H. Dunning, and R. J. Harrison, J. Chem. Phys. **96**, 6796–6806 (1992).

[45]M. J. Frisch, G. W. Trucks, H. B. Schlegel, G. E. Scuseria, M. A. Robb, J. R. Cheeseman, G. Scalmani, V. Barone, B. Mennucci, G. A. Petersson, H. Nakatsuji, M. Caricato, X. Li, H. P. Hratchian, A. F. Izmaylov, J. Bloino, G. Zheng, J. L. Sonnenberg, M. Hada, M. Ehara, K. Toyota, R. Fukuda, J. Hasegawa, M. Ishida, T. Nakajima, Y. Honda, O. Kitao, H. Nakai, T. Vreven, J. A. Montgomery, Jr., J. E. Peralta, F. Ogliaro, M. Bearpark, J. J. Heyd, E. Brothers, K. N. Kudin, V. N. Staroverov, R. Kobayashi, J. Normand, K. Raghavachari, A. Rendell, J. C. Burant, S. S. Iyengar, J. Tomasi, M. Cossi, N. Rega, J. M. Millam, M. Klene, J. E. Knox, J. B. Cross, V. Bakken, C. Adamo, J. Jaramillo, R. Gomperts, R. E. Stratmann, O. Yazyev, A. J. Austin, R. Cammi, C. Pomelli, J. W. Ochterski, R. L. Martin, K. Morokuma, V. G. Zakrzewski, G. A. Voth, P. Salvador, J. J. Dannenberg, S. Dapprich, A. D. Daniels, Ö. Farkas, J. B. Foresman, J. V. Ortiz, J. Cioslowski, and D. J. Fox, GAUSSIAN 09, Revision A.03, Gaussian, Inc., Wallingford, CT, 2009.

[46]S. J. Klippenstein, L. B. Harding, and B. Ruscic, J. Phys. Chem. A **121**, 6580–6602 (2017).

[47]B. O. Roos, P. Linse, P. E. M. Siegbahn, and M. R. A. Blomberg, Chem. Phys. **66**, 197–207 (1982).

[48]K. Andersson, P. A. Malmqvist, B. O. Roos, A. J. Sadlej, and K. Wolinski, J. Phys. Chem. **94**, 5483–5488 (1990).

[49]K. Andersson, P. Å. Malmqvist, and B. O. Roos, J. Chem. Phys. **96**, 1218–1226 (1992).

[50]T. H. Dunning, J. Chem. Phys. **90**, 1007–1023 (1989).

[51]H.-J. Werner, P. J. Knowles, G. Knizia, F. R. Manby, M. Schütz, P. Celani, W. Györffy, D. Kats, T. Korona, R. Lindh, A. Mitrushenkov, G. Rauhut, K. R. Shamasundar, T. B. Adler, R. D. Amos, A. Bernhardsson, A. Berning, D. L. Cooper, M. J. O. Deegan, A. J. Dobbyn, F. Eckert, E. Goll, C. Hampel, A. Hesselmann, G. Hetzer, T. Hrenar, G. Jansen, C. Köppl, Y. Liu, A. W. Lloyd, R. A. Mata, A. J. May, S. J. McNicholas, W. Meyer, M. E. Mura, A. Nicklaß, D. P. O'Neill, P. Palmieri, D. Peng, K. Pflüger, R. Pitzer, M. Reiher, T. Shiozaki, H. Stoll, A. J. Stone, R. Tarroni, T. Thorsteinsson, M. Wang, and M. Welborn, MOLPRO, version 2015.1, a package of *ab initio* programs, 2015, see http://www.molpro.net.

[52]B. Marchetti, T. N. V. Karsili, M. Ciprian, C. S. Hansen, and M. N. R. Ashfold, J. Chem. Phys. **147**, 013923 (2017).

[53]C. Yin and K. Takahashi, Phys. Chem. Chem. Phys. **20**, 16247–16255 (2018).

[54]M. Barbatti, G. Granucci, M. Persico, M. Ruckenbauer, M. Vazdar, M. Eckert-Maksić, and H. Lischka, J. Photochem. Photobiol., A **190**, 228–240 (2007).

[55]M. Barbatti, A. J. A. Aquino, and H. Lischka, Phys. Chem. Chem. Phys. **12**, 4959–4967 (2010).

[56]M. Barbatti, M. Ruckenbauer, F. Plasser, J. Pittner, G. Granucci, M. Persico, and H. Lischka, Wiley Interdiscp. Rev. Comput. Mol. Sci. **4**, 26–33 (2014).

[57]T. N. V. Karsili, B. Marchetti, and M. N. R. Ashfold, Dalton Trans. **45**, 18921–18930 (2016).

[58]T. N. V. Karsili, M. Thodika, L. Nguyen, and S. Matsika, Chem. Phys. **515**, 434–440 (2018).

[59]A. D. Becke, J. Chem. Phys. **98**, 5648–5652 (1993).

[60]R. Krishnan, J. S. Binkley, R. Seeger, and J. A. Pople, J. Chem. Phys. **72**, 650–654 (1980).

[61]J. H. Lehman, H. Li, J. M. Beames, and M. I. Lester, J. Chem. Phys. **139**, 141103 (2013).

[62]S. T. Pratt, P. M. Dehmer, and J. L. Dehmer, Phys. Rev. A **43**, 4702–4711 (1991).

[63]G. A. Garcia, L. Nahon, and I. Powis, Rev. Sci. Instrum. **75**, 4989–4996 (2004).

[64]K. S. Dooley, J. N. Geidosch, and S. W. North, Chem. Phys. Lett. **457**, 303–306 (2008).

[65]D. H. Mordaunt, D. L. Osborn, and D. M. Neumark, J. Chem. Phys. **108**, 2448–2457 (1998).

[66]D. J. Hadden, G. M. Roberts, T. N. Karsili, M. N. Ashfold, and V. G. Stavros, Phys. Chem. Chem. Phys. **14**, 13415–13428 (2012).

[67]F. Liu, J. M. Beames, A. S. Petit, A. B. McCoy, and M. I. Lester, Science **345**, 1596–1598 (2014).

[68]Y. Fang, F. Liu, S. J. Klippenstein, and M. I. Lester, J. Chem. Phys. **145**, 044312 (2016).

[69]F. Liu, J. M. Beames, and M. I. Lester, J. Chem. Phys. **141**, 234312 (2014).